The 2005 HST Calibration Workshop
Space Telescope Science Institute, 2005
A. M. Koekemoer, P. Goudfrooij, and L. L. Dressel, eds.

Correcting STIS CCD Point-Source Spectra for CTE Loss[1]

Paul Goudfrooij, Ralph C. Bohlin, and Jesús Maíz-Apellániz[2]

Space Telescope Science Institute, 3700 San Martin Drive, Baltimore, MD 21218

Abstract. We review the on-orbit spectroscopic observations that are being used to characterize the Charge Transfer Efficiency (CTE) of the STIS CCD in spectroscopic mode. We parametrize the CTE-related loss for spectrophotometry of point sources in terms of dependencies on the brightness of the source, the background level, the signal in the PSF *outside the standard extraction box*, and the time of observation. Primary constraints on our correction algorithm are provided by measurements of the CTE loss rates for simulated spectra (images of a tungsten lamp taken through slits oriented along the dispersion axis) combined with estimates of CTE losses for actual spectra of spectrophotometric standard stars in the first order CCD modes. For point-source spectra at the standard reference position at the CCD center, CTE losses as large as 30% are corrected to within $\sim$1% RMS after application of the algorithm presented here, rendering the Poisson noise associated with the source detection itself to be the dominant contributor to the total flux calibration uncertainty.

1. Introduction

Since the installation of the Space Telescope Imaging Spectrograph (STIS) onto HST in February 1997, radiation damage to its CCD (which is primarily due to high-energy protons which are especially abundant when crossing the South Atlantic Anomaly) has caused a degradation of its Charge Transfer Efficiency (CTE, defined as the fraction of charge transferred from one pixel to the next during readout). In characterizing the effect of the radiation damage to CCD performance it is often more useful to use the term Charge Transfer *Inefficiency* (CTI = 1−CTE). The observational effect of CTI is that an object whose induced charge has to traverse many pixels before being read out appears to be fainter than the same object observed near the read-out amplifier.

Earlier on-orbit characterizations of the CTI of the STIS CCD have mostly concentrated on the (time-dependent) effect on imaging photometry of point sources of varying signal and background levels as well as measurement aperture sizes (Gilliland, Goudfrooij, & Kimble 1999; Kimble, Goudfrooij, & Gilliland 2000; Goudfrooij & Kimble 2003). However, the CTI corrections reported in those papers are not applicable to spectroscopic observations since the charge structure of spectral data is significantly different from that of imaging exposures. This is illustrated in Figure 1. Consider STIS observations, where the spectral dispersion direction is along rows and the parallel readout direction[3] is along columns. Then, for a given signal level in a measurement element, imaging data features a significantly different signal in each column, whereas spectroscopic data is much more constant along rows. As

[1]Based on observations with the NASA/ESA *Hubble Space Telescope*, obtained at the Space Telescope Science Institute, which is operated by AURA, Inc., under NASA contract NAS5-26555

[2]Affiliated with the Space Telescope Division, European Space Agency

[3]The CTI of the STIS CCD is only significant in the parallel readout direction (e.g., Kimble et al. 2000). Hence, this paper only addresses *parallel* CTI.

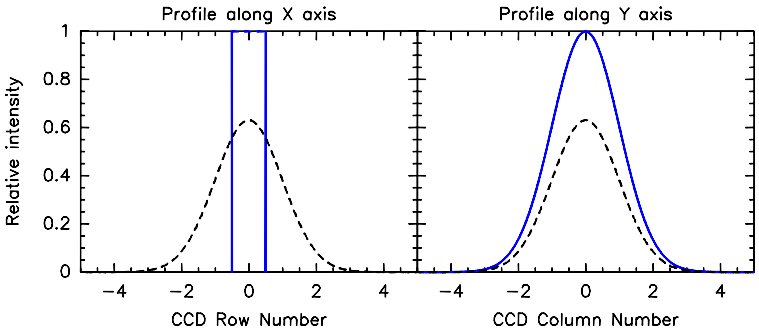

Figure 1: Illustration of the difference in charge structure between imaging and spectroscopic data. The dispersion direction for the latter is assumed to be along rows. For a given signal level per measurement element (per pixel along the dispersion for spectra, per object within a circular aperture for imaging data), spectroscopic data (solid lines) have a higher signal level per column than imaging data (dashed lines). Since the STIS CCD virtually only suffers from CTI in the parallel read-out direction (along the Y axis), this results in a lower CTI for spectroscopic vs. imaging data of a given total measured signal level.

the CTI is highly dependent on signal level and the ratio between background and signal level (see below), this leads to significantly different CTI values for a given total signal.

The purpose of the current paper is to characterize the CTI of the STIS CCD for point-source spectrophotometry in terms of its dependencies on signal level within the spectrum extraction box, background counts outside the extraction box, and elapsed on-orbit time. The results described in this paper supersede those reported in an earlier STIS Instrument Science Report (Bohlin & Goudfrooij 2003, hereafter BG03).

The STIS CCD is a 1024×1024 pixel, backside-illuminated device with $21\,\mu\mathrm{m} \times 21\,\mu\mathrm{m}$ pixels. It was fabricated by Scientific Imaging Technology (SITe) with a coating process that allows it to cover the $200-1000$ nm wavelength range for STIS in a wide variety of imaging and spectroscopic modes. Two serial registers are available. Read-out amplifiers are located at all four corners, each with an independent signal processing chain. By default, science exposures employ full-frame readout through amplifier 'D' (located at the top right of the CCD), which features the lowest read-out noise. Further technical details regarding the STIS CCD are provided in Kimble et al. (1994, 2000).

This paper is organized as follows. Section 2 describes the method used to derive the time constant of the CTI of the STIS CCD in spectroscopic mode. We derive functional dependencies of the spectroscopic CTI on source counts, background counts, and spatial extent of the point-spread function (PSF) in Section 3. We end with concluding remarks.

2. The Time Constant of the CTI of the STIS CCD

We derive the time constant of the CTE degradation of the STIS CCD using a method designated the "Internal Sparse Field" test, which provides measurements that are directly applicable to spectroscopic observations with the STIS CCD. This test was developed by the STIS Instrument Definition Team during ground calibration, and it has been used throughout the on-orbit lifetime of STIS to allow accurate monitoring. It quantifies two key aspects of CTE effects on spectroscopic measurements: *(i)* The amount of charge lost *outside* a standard extraction aperture, and *(ii)* the amount of centroid shift experienced

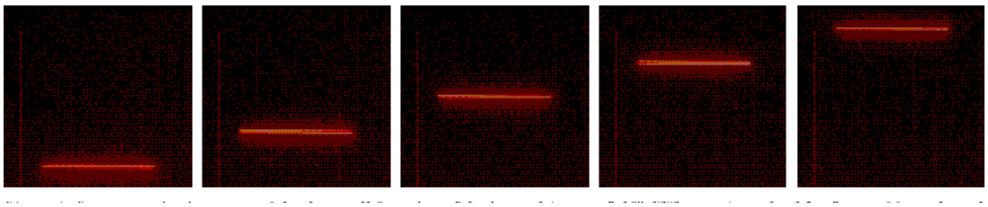

Figure 2: Representative images used for the parallel version of the "Internal Sparse Field" CTE test. A sequence of exposures is taken at each of five positions along the CCD columns, alternating between read-out amplifiers 'D' (located at top right) and 'B' (at bottom right). Systematic variation of the relative intensities observed by the two amplifiers as a function of position reveals the CTE effect (see Fig. 3).

by the charge that remains *within* that extraction aperture. The "internal"[4] version of the sparse field test was implemented as follows. Using an onboard tungsten lamp, the image of a narrow slit is projected at five positions along the CCD columns. At each position, a sequence of exposures is taken, alternating between the 'B' and 'D' amplifiers for readout. This is illustrated in Figure 2. For each exposure, the average flux per column within a 7-row extraction aperture (i.e, the default extraction size for long-slit STIS spectra of point sources, cf. Leitherer & Bohlin 1997) as well as the centroid of the image profile within those 7 rows are calculated. The alternating exposure sequence allows one to separate CTE effects from flux variations produced by warmup of the tungsten lamp. As the slit image extends across hundreds of columns, high statistical precision on CTE values can be obtained even at low signal levels per column. Although these data are not necessarily taken in dispersed mode[5], the illumination is representative for typical spectroscopic observations (as the dispersion direction of STIS CCD spectral modes is along rows). The slit image has a narrow profile (2-pixel FWHM), similar to a point source spectrum.

A key virtue of this method is that neither a correction for flat-field response non-uniformity is required, nor an a-priori knowledge of the source flux (as long as the input source is stable during the alternating exposures). It should be noted that what is being measured is actually a sum of the charge transfer inefficiencies for the two different clocking directions. However, given the identical clocking voltages and waveforms and with the expected symmetry of the radiation damage effects, we believe the assumption that the CTI is equal in the two different directions is a reasonable one.

We emphasize that in calculating CTI from this test, charge is only considered "lost" if it is no longer within the standard 7-row extraction aperture. I.e., we are only measuring the component of CTI produced by relatively long-time-constant charge trapping. Hence, the CTI values derived from this test will not agree with those measured by (e.g.) X-ray stimulation techniques using Fe^{55} or Cd^{109}, for which charge deferred to even the very first trailing pixel formally contributes to the CTI. However, the measurement described here *is* directly relevant to the estimation of CTE effects on STIS spectrophotometry.

2.1. Results

A χ^2-minimization algorithm was used to compute CTI for each observing epoch and signal level. After correcting for (small) gain differences in the two readout amplifier chains, the

[4] "Internal" in this context means that the necessary observations were performed during Earth occultations, hence not requiring any valuable "external" *HST* observing time

[5] About half of the exposures employ STIS in imaging mode using a mirror in the mode select mechanism; the other half use the G430M grating at central wavelength 5471 Å, which produces a very flat spectrum when used with the Tungsten lamp.

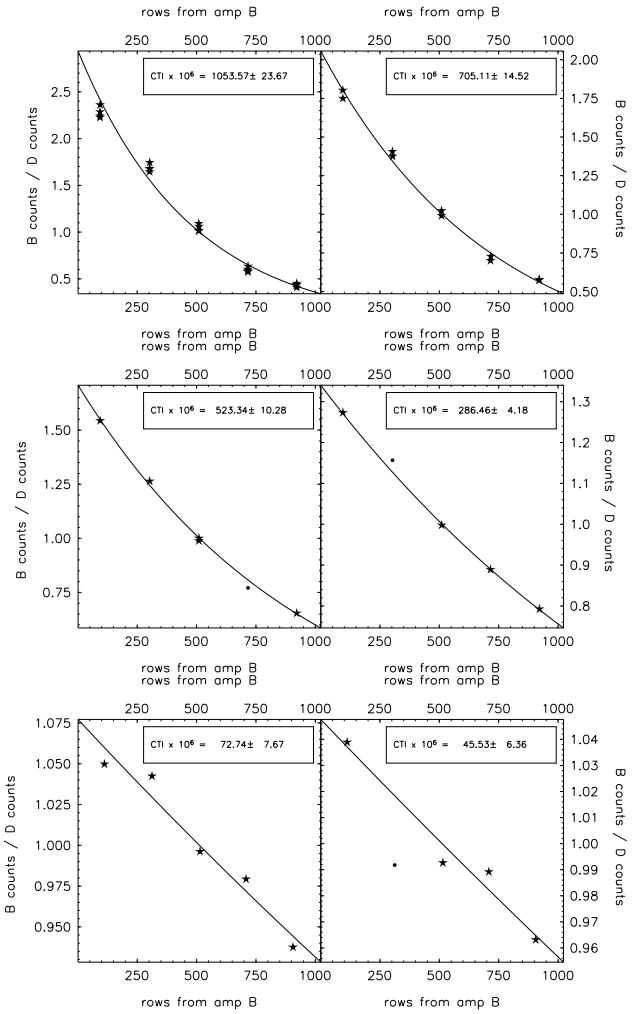

Figure 3: CTI calculation for the internal sparse field measurements of September 2003. Each panel shows the data and the fit for a given signal level. For the panels from the upper left through the upper right, middle left, etc., the signal levels are 60, 130, 195, 500, 3450, and 9850 e^-, respectively. Star symbols indicate measurements used in the fit and circles indicate rejected points. Fitted CTI values are indicated in the boxed legend.

observed ratio of the fluxes measured by the two amps was fit to a simple CTE model of constant fractional charge loss per pixel transfer, allowing for $\kappa - \sigma$ clipping of outliers (the latter arise occasionally from lamp intensity fluctuations of short (0.2 sec) exposures). Flux ratio results for the parallel internal sparse field test taken in `CCDGAIN=1` after 5.5 years in orbit are presented in Figure 3. It can be seen that this simple CTE model fits the data as a function of source position along the parallel clocking direction of the CCD quite well.

To derive the time dependence of the CTI, all CTI measurements were first normalized to a constant background value, i.e. zero background. In order to arrive at that value, two corrections were required: First, the effect of the spurious charge in STIS CCD bias frames (Goudfrooij & Walsh 1997) was accounted for by considering the total background to be the measured one plus the spurious charge. Second, the background dependency of the CTI (to be described in Section 3 below) was taken into account.

CTI values derived as mentioned above for the parallel internal sparse field test taken at different epochs are plotted in Figure 4. In-flight CTE degradation from a pre-flight starting point of low CTI is obvious. Typical CTI behavior is observed as a function of

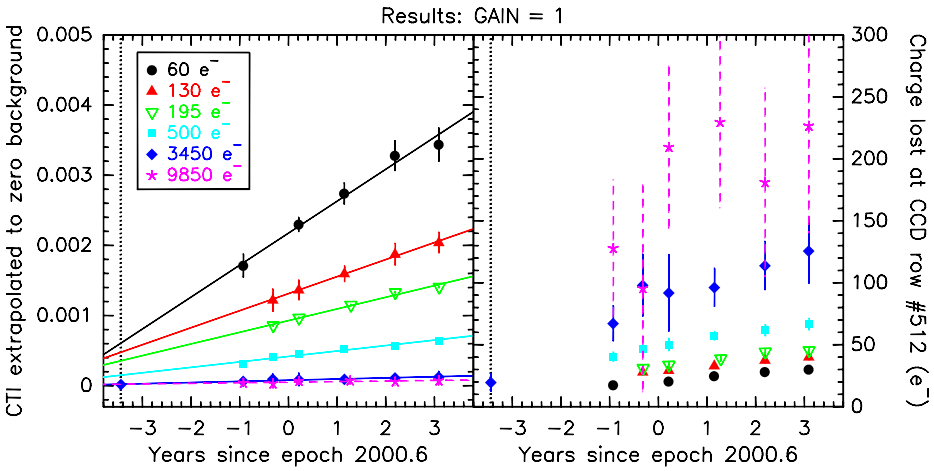

Figure 4: *Left panel:* CTI extrapolated to zero background for `CCDGAIN=1` as a function of time and signal level, derived from the internal sparse field test. Both the data and the corresponding linear fits are plotted. Symbols associated with individual signal levels (corrected for CTI) are indicated in the legend. *Right panel:* Absolute charge lost due to CTI for an object at the central row of the STIS CCD as a function of time and signal level. Symbol types are the same as in the left panel. The epoch of HST Servicing Mission 2 (during which STIS was installed on HST) is depicted as a vertical black dotted line.

signal level: The *fractional* charge loss (which is proportional to CTI) drops with increasing signal level, while the *absolute* level of charge loss increases. The time dependence was derived by fitting the zero-background CTI values to a function of the form:

$$\mathrm{CTI}(t) = \mathrm{CTI}(0)\,[1 + \alpha(t - t_0)], \tag{1}$$

with t in years and $t_0 = 2000.6$, the approximate midpoint in time of in-flight STIS observations.

Results for the time-dependence fit for the `CCDGAIN=1` setting are shown in Fig. 4 and Table 1. The functional fit to the data is quite good, and the derived values for α in Eq. (1) are consistent with one another (within the uncertainties) for all signal levels measured. As to the selection of the time constant α, we considered that the dataset with 3450 electrons per column is the only one for which pre-flight measurements were available, i.e., it covers a time interval considerably longer than for the other signal levels. Hence time constant $\alpha = 0.218 \pm 0.038$ was selected as representative for all signal levels, as indicated in Table 1.

Table 1: CTE degradation time constant α as a function of signal level for `CCDGAIN=1`. The last row lists our adopted value in boldface font.

signal (e^-)	α (yr^{-1})	σ_α (yr^{-1})
60	0.216	0.009
130	0.192	0.013
195	0.188	0.011
500	0.202	0.006
3450	0.218	0.038
9850	0.170	0.052
α = **0.218 ± 0.038**		

3. Insights on CTI From Monitoring of Flux Standard Star Spectra

3.1. Methodology to derive dependence on signal and background levels

The CTI values derived from the internal sparse field test are "worst-case", since there is essentially no background intensity ("sky" or dark current) to provide filling of charge traps in the silicon lattice of the CCD. Hence, additional observations are needed to constrain the functional dependence of CTI on the background and signal levels. For this purpose we build upon the work of BG03 who utilized the large database of spectrophotometric standard star spectra taken on a regular basis (every few months) using a 2 arcsec wide slit. CTI values for spectra of DA white dwarf flux standards GD 71 and LDS 749B taken using the G230LB and G430L gratings are calculated by dividing their measured fluxes by those measured from G230L spectra taken within a few *HST* orbits from one another. The (time-dependent) flux calibration for the G230L mode (which uses the NUV-MAMA detector, which does *not* suffer from CTE loss) is very well established, and accurate to subpercent level (Stys, Bohlin, & Goudfrooij 2004). The standard star spectra used to characterize the CTI effects are listed in Table 2 along with their signal and background levels.

Table 2: List of flux standard star spectra used to characterize CTI effect as function of signal and background level per exposure. All intensities are in e^-.

Rootname	Grating	Flux Standard	Background level	Range in Signal Levels
o6ig10010	G230LB	G191-B2B	0.4	1000 – 5000
o6ig100d0	G750L	G191-B2B	0.5	150 – 7900
o6il01020	G230LB	LDS 749B	1.9	100 – 1800
o8u2200b0	G430L	AGK+81D266	0.5	3000 – 9200
o8v101030	G750L	WD 1657+343	2.5	30 – 750
o8v2040e0	G230LB	GD 71	0.3	120 – 730
o8v204030	G230LB	GD 71	0.1	20 – 170

In evaluating a suitable functional form to characterize the CTI of the STIS CCD in spectroscopic mode, BG03 followed Goudfrooij & Kimble (2003) who showed that the logarithm of CTI scales roughly linearly with the logarithm of the signal level in imaging mode (a glance at panels (b) and (d) in Figure 7 of the current paper shows the same is true for the spectroscopic modes), and that the slope of log (CTI) vs. log (background) decreases systematically with increasing source signal level[6], suggesting a functional form similar to CTI $\propto \beta\, G^{-\gamma}\ \exp(-\delta[B/G]^{\epsilon})$ where B is the background level and G is the gross signal level. After making initial estimates of parameters β through ϵ from bootstrap tests and using the CTI time constant as it was determined in the spring of 2003 ($\alpha = 0.243 \pm 0.042$), BG03 determined a best-fit functional form

$$CTI(B,G,t) = 0.0355\ G^{-0.750}\ (0.243(t-2000.6)+1)\ \exp(-2.97\,(B'/G)^{0.21}) \qquad (2)$$

where B' is the sum of the sky B, the dark current, and the spurious charge (which are all included in G as well). The values for B and G are readily obtained from the output of the X1D routine within CALSTIS to extract 1-D spectra (McGrath, Busko, & Hodge 1999). The efficacy of the correction per Eq. (2) in removing the CTI effect is illustrated in Figure 5. CTI-induced flux errors as high as $\sim$15-20% at low signal levels (~ 100 – 150 e^- per 7-pixel extraction) are reduced to $\lesssim 1.5\%$ by applying Eq. (2), i.e., an improvement of a factor 10.

[6] A likely physical explanation of this effect is that the background charge fills relatively more traps for small charge packets being clocked through than it does for large charge packets.

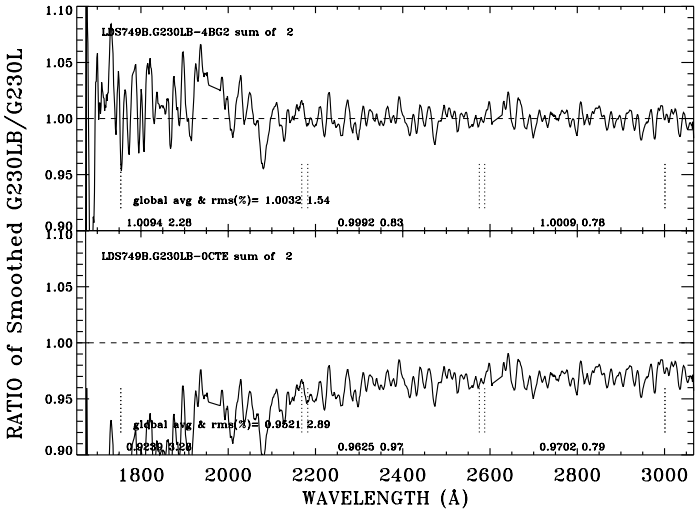

Figure 5: Ratio of the CCD/G230LB flux to the MAMA/G230L flux for LDS 749B. The CCD/G230LB signal level ranges between ~ 90 and 1800 e^-. Both denominator and numerator have been corrected for similar changes of sensitivity with time as per Stys et al. (2004). The bottom panel reveals the G230LB flux error before any CTI correction is applied; the top panel shows the residuals after application of the BG03 CTI algorithm. The global value and rms of the residuals are written on each panel, along with three mean and rms values for the three separate regions delineated by the vertical dashed lines. The bottom panel shows that the error of 8% (0.9229) before CTI correction in the shortest-wavelength region is reduced to $\sim 1\%$ (1.0094) after CTI correction.

3.2. The Impact of the "Red Halo" of the PSF of the STIS CCD

The CTI correction algorithm derived by BG03 was implemented in the CALSTIS pipeline by December 16, 2003, and it still is active at the time of writing. Recently, further testing has shown that application of the BG03 algorithm yields systematic residuals at the red end of the wavelength range covered by the G750L grating. The PSF of the STIS CCD features broad wings at wavelengths $\gtrsim$ 7500 Å (Leitherer & Bohlin 1997), the width of which increases strongly with increasing wavelength. This "red halo" is believed to be due to scatter within the CCD mounting substrate which becomes more pronounced as the silicon transparency increases at long wavelengths. The effects of the red halo are significant, particularly beyond 9500 Å where the default 7-pixel extraction box captures only $\lesssim 70\%$ of the light in the PSF.

This extended halo is likely to have a significant effect on the CTI experienced by the signal within the default 7-pixel extraction box, as the charge induced by the halo acts effectively as 'background' in filling traps. However, the red halo signal is not currently included in the background term (B' in Eq. 2), since the background spectrum used within CALSTIS/X1D is taken far away from the spectrum location[7]. To resolve this issue, we have devised the following update to the CTI correction algorithm of BG03. We split up the background term in two separate terms, B' (as before) and a new term H which contains the fraction of PSF signal *above* the default 7-pixel extraction box. Fortunately, values for H as a function of wavelength can be derived from existing CALSTIS reference files (namely

[7]300 unbinned CCD pixels away by default, as listed in the BK1OFFST and BK2OFFST columns in the 1-D Extraction Parameters Table Reference File, which is listed in data header keyword XTRACTAB.

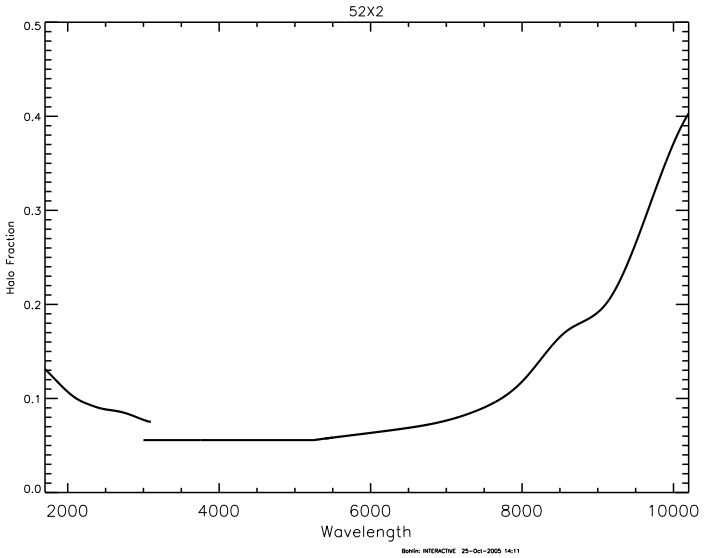

Figure 6: Parameter H in Eq. 4: The fraction of the light in the PSF outside the default 7-pixel extraction box, as a function of wavelength for CCD grating modes. Note the discontinuity near 3000 Å, at the boundary of the wavelength ranges covered by the G230LB and G430L gratings. This is likely due to the presence of a Lyot stop in the G430L and G750L modes which is absent in the G230LB mode (see also contributions of L. Dressel and C. Proffitt in this volume).

from the Photometric Correction Tables[8]). We plot these H values in Figure 6. H is non-negligible at any wavelength, but the spatial extent of the PSF beyond the default extraction box is only a few CCD pixels below $\sim$8000 Å. Hence, low values of H do not necessarily lower the CTI significantly. This effect is accounted for by subtracting a certain minimum threshold value from the measured value of H (i.e., parameter η below).

Considering all of the above, the new functional form of the CTI algorithm is

$$\begin{aligned} \mathrm{CTI} &= (\alpha(t-2000.6)+1)\,\beta\,G^{-\gamma}\,\exp(-\delta[(B'+\epsilon H')/G]^{\zeta}) \\ \text{where } H' &= \max(0.0,(H-\eta))\times Net. \end{aligned} \tag{3}$$

($Net = G-7B$, the net counts in the spectrum.) Initial estimates of the values of parameters β through η and their uncertainties were made using bootstrap tests. A robust fit parameter was then minimized using a non-linear minimization routine from *Numerical Recipes* (Press et al. 1992). Best-fit values of the parameters β through η are listed in Table 3.

The quality of this parametrization of the CTI correction is illustrated in Figure 7, along with a comparison to the BG03 algorithm. Comparing panels (c) and (e) in particular, it is clear that the new solution yields a significantly better correction for the red end of G750L spectra, especially for that of the faint white dwarf WD1657+343 (rootname `o8v101030`). Application of the new CTI correction also renders the STIS G750L fluxes of all faint standards used to determine the apparent NICMOS non-linearity (Bohlin et al. 2005; de Jong et al. 2006, this volume) to be consistent with the relation depicted in Fig. 3 of Bohlin et al. (2005), which lends support to the correctness of the new algorithm. The only spectrum tested for which the new solution still yields a significant residual ($\sim$1%) is the short (35 s) G750L exposure of the DA0 white dwarf G191-B2B (rootname `o6ig100d0`). However, that spectrum shows a 1% error for *any* CTI model at the bright, blue end of the G750L

[8] `*_pct.fits`, listed in data header keyword PCTAB.

Table 3: Best-fit Values of Coefficients in CTI Functional Form (Eq. 4).

Coefficient	Value	Description
α	0.218 ± 0.038	Time dependence of CTI
β	0.056 ± 0.001	CTI normalization
γ	0.82 ± 0.01	Gross count level dependence
δ	3.00 ± 0.05	Normalization for 'background'/gross count ratio
ϵ	1.30 ± 0.10	Multiplicative factor for halo light fraction
ζ	0.18 ± 0.01	Power of 'background'/gross count ratio
η	0.06 ± 0.01	Minimum value of halo light fraction above spectrum

wavelength range, which is unlikely to be due to CTI effects since the CTI algorithm works very well for the other spectra at the same signal and background levels. Furthermore, the new CTI algorithm renders this 1% error to be virtually independent of wavelength for G191-B2B, which again supports the algorithm's correctness.

Overall, the new CTI parametrization formula yields a correction that is accurate within 5% for any data point, while the RMS accuracy for all spectra used in this study stays within 1%. For reference, the dotted lines in panel (e) in Figure 7 show the Poisson noise associated with a resolution element (assumed to be 2 pixels along the dispersion) in spectra of a given signal level. *The new CTI correction formula renders flux calibration to an accuracy better than the uncertainty due to Poisson noise.*

4. Concluding Remarks

We have reviewed the methods used for empirical characterization of the CTI of the STIS CCD and its evolution, using both internal and external exposures which provide measures that are directly applicable to typical spectroscopic observations with the STIS CCD. We derived a functional form for the CTI correction in a semi-empirical fashion, taking into account dependencies on signal level, background level, and the charge trap filling effect of the extended halo in the PSF of the STIS CCD redward of ~ 7500 Å. After applying this CTI correction formula to observed data, systematic residuals stay within 1% (RMS).

The revised CTI correction algorithm presented in this paper will be implemented within the CALSTIS/OTFR pipeline by the next applicable OTFR build. As always, researchers using STIS will be kept in touch on STIS calibration updates like this by email, through the *Space Telescope Analysis Newsletter* which is also available through the "Document Archive" section of the STIS website at `http://www.stsci.edu/hst/stis`.

Acknowledgments. We acknowledge useful discussions with Paul Bristow and invite readers to check out his paper in this volume (Bristow, Kerber, and Rosa 2006), presenting a more physically based CTE correction method for the STIS CCD. We thank Rossy Diaz-Miller for her help in doing tests of the Bristow method and comparisons of its results with those of the empirical method described here.

References

Bohlin, R. C., & Goudfrooij, P., 2003, *Instrument Science Report* STIS 2003-03 (Baltimore: STScI) (BG03), available through http://www.stsci.edu/hst/stis

Bohlin, R. C, Lindler, D. J., & Riess, A., 2005, *Instrument Science Report* NICMOS 2005-02 (Baltimore: STScI), available through http://www.stsci.edu/hst/nicmos

Bristow, P., Kerber, F., Rosa, M.R., 2006, The 2005 *HST Calibration Workshop.* Eds. A. M. Koekemoer, P. Goudfrooij, & L. L. Dressel, this volume

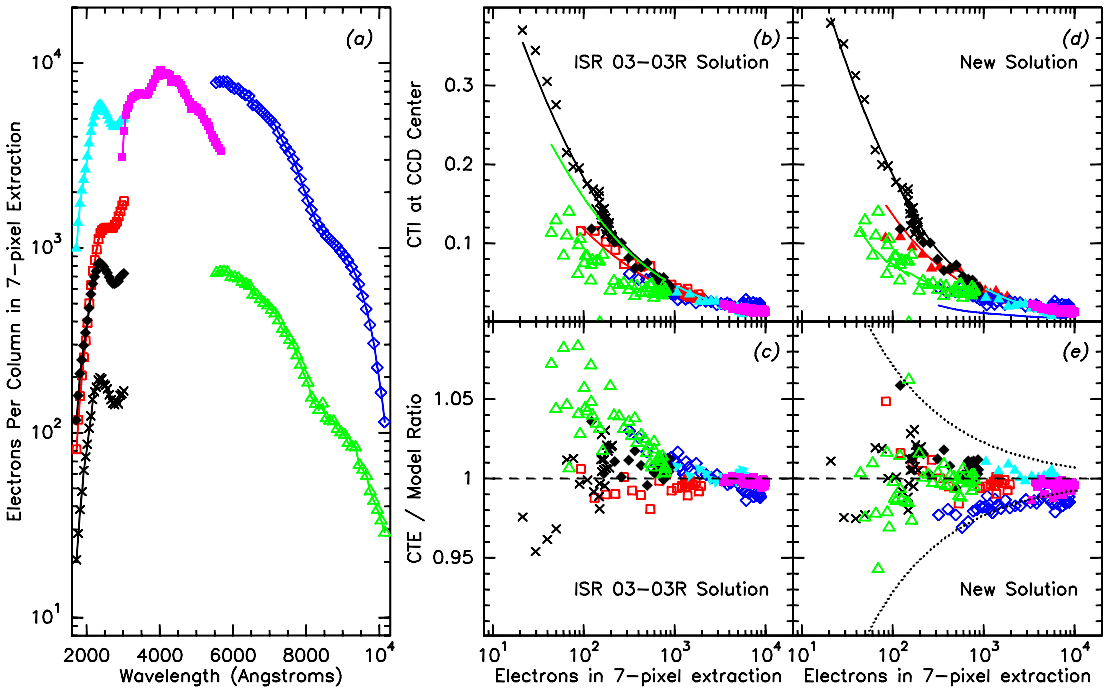

Figure 7: *Panel (a):* Smoothed flux standard star spectra used to determine the functional form of the CTI of the STIS CCD in spectroscopic mode. *Panel (b):* CTI at the central row of the CCD vs. gross signal level within the default 7-pixel extraction box. Symbols represent measured CTI values for the spectra shown in panel (a) using the CTI time constant as determined by BG03 at the time. The drawn lines represent the predictions of the model by BG03 for those data. Symbol types are the same as in panel (a). *Panel (c):* The ratio of measured CTE values and the model predictions by BG03 vs. gross signal level. *Panel (d):* Same as panel (b), but using the CTI time constant and functional form determined in this paper (i.e., Eq. 4). *Panel (e):* Same as panel (c), but using the CTI time constant and functional form determined in this paper. For reference, the dotted lines delineate the uncertainty due to Poisson noise associated with a resolution element of a spectrum with the given signal level.

Gilliland, R. L., Goudfrooij, P., & Kimble, R. A., 1999, PASP, 111, 1009

Goudfrooij, P., & Walsh, J. R., 1997, *Instrument Science Report* STIS 1997-09 (Baltimore: STScI)

Goudfrooij, P., & Kimble, R. A., 2003, in *Proc. 2002 HST Calibration Workshop*, ed. S. Arribas, A. Koekemoer, & B. Whitmore (Baltimore: STScI), p. 105

Kimble, R. A., Brown, L., Fowler, W. B., Woodgate, B. E., Yagelowich, J. J., et al., 1994, Proc. SPIE, 2282, p. 169

Kimble, R. A., Goudfrooij, P., & Gilliland, R. L., 2000, Proc. SPIE, 4013, p. 532

Leitherer, C., & Bohlin, R. C., 1997, *Instrument Science Report* STIS 97-13 (Baltimore: STScI)

McGrath, M. A., Busko, I., & Hodge, P., 1999, *Instrument Science Report* STIS 1999-03 (Baltimore: STScI)

Press, W. H., Flannery, B. P., Teukolsky, S. A., & Vetterling, W. T., 1992, Numerical Recipes in Fortran (Cambridge: Cambridge University Press)

Stys, D. J., Bohlin, R. C., & Goudfrooij, P., 2004, *Instrument Science Report* STIS 2004-04 (Baltimore: STScI)